AGU PUBLICATIONS

JGR

Journal of Geophysical Research: Solid Earth

RESEARCH ARTICLE
10.1002/2015JB012364

Key Points:
- Geysers can be hydraulically connected through permeable pathways to other hot springs
- The level of complexity of geyser eruptions may be controlled by the underground geometry
- Over time geysers change periodicity, develop new thermal features, and shift interactions

Supporting Information:
- Movie S1
- Movie S2
- Captions for Movies S1 and S2

Correspondence to:
C. Munoz-Saez,
carolimunoz@berkeley.edu

Citation:
Munoz-Saez, C., A. Namiki, and M. Manga (2015), Geyser eruption intervals and interactions: Examples from El Tatio, Atacama, Chile, *J. Geophys. Res. Solid Earth*, *120*, doi:10.1002/2015JB012364.

Received 16 JUL 2015
Accepted 5 OCT 2015
Accepted article online 1 OCT 2015

Geyser eruption intervals and interactions: Examples from El Tatio, Atacama, Chile

Carolina Munoz-Saez[1], Atsuko Namiki[2], and Michael Manga[1]

[1]Department of Earth and Planetary Science, University of California, Berkeley, California, USA, [2]Hiroshima University, Hiroshima, Japan

Abstract We compare and contrast data collected in 2012 and 2014 from the El Tatio geyser field, Chile. We identify geyser systems that evolve over time, including changes in the interval between eruptions, development of new thermal features, and interactions between geysers. We study three different cases: (a) an isolated geyser, which is periodic and has nearly identical eruptions every cycle; (b) a geyser and coupled noneruptive pool, where the geyser has nonregular cycles and several preplay eruptions before the main eruption; and (c) two geysers and a mud volcano, which have nonregular cycles and are all interacting. Though geysers erupt with different styles, we recognize some common features: the conduit recharges with liquid during the quiescent period, bubbles enter the conduit before eruptions, and eruptions occur when water boils in the upper part of the conduit. The episodic addition of heat may govern the periodicity, while the depth where heat is added dictates the eruption style: conduits with deeper heat input are more likely to show preplay or minor eruptions. The interactions between thermal features can be explained by pressure transmission in subsurface permeable layers between geyser conduits.

1. Introduction

Geysers are eruptive hot springs that episodically discharge steam, liquid water, and noncondensable gases. Most geysers on Earth are concentrated in Yellowstone National Park (United States), Geyser Valley (Russia), and El Tatio (Chile). Formation of geysers in these areas is due to particular combinations of water supply, heat sources, and fractures and/or porous rocks [e.g., *White*, 1967; *Fournier*, 1969; *Kieffer*, 1989; *Ingebritsen and Rojstaczer*, 1993, 1996; *Kedar et al.*, 1998; *Kiryukhin et al.*, 2012].

Subsurface geometry and fluid flow pathways may govern eruption characteristics. Conduits and reservoirs in the geysers system may have a complex geometry [*Hutchinson et al.,* 1997]. Cavities underneath geysers may act as "bubble traps," accumulating liquid and steam [*Belousov et al.*, 2013]. The episodic release of fluid from the cavities can be linked to the periodicity of eruptions [*Mackenzie*, 1811; *Belousov et al.*, 2013; *Vandemeulebrouck et al.*, 2013; *Adelstein et al.*, 2014; *Munoz-Saez et al.*, 2015]. Bubbles of steam can also transfer enough heat to warm water in the conduit and permit sustained eruptions [*Kieffer*, 1984, 1989; *Adelstein et al.*, 2014]. Geysers may also be hydraulically connected with other nearby thermal springs [e.g., *Scott*, 1992, 1994], and diffusion of fluid pressure changes may be responsible for the communication between geysers [*Rojstaczer et al.*, 2003].

There remain open questions about the geometry beneath geysers and their interaction with other springs: How is the eruption cycle of a geyser influenced by other adjacent and distant thermal sources? Are hot springs and geysers connected through permeable pathways? Why do so few hot springs erupt as geysers?

We studied geysers whose eruption characteristics evolve over time and that interact with those of other hot springs or geysers. During 1 week periods in October 2012 and October 2014, we made measurements at three different geysers that display differing degrees of complexity in their eruption cycles: (1) an isolated geyser that erupted regularly, called El Jefe (EJ), representing the simplest case; (2) a geyser that interacts with an adjacent thermal pool, called Vega Rinconada geyser (VRG) and Vega Rinconada pool (VRP), respectively; and (3) a geyser that in 2012 was an independent single system called El Cobreloa geyser (CL) but in 2014 was found interacting with a secondary geyser called El Cobresal (CS) and a mud volcano (MV). In 2012, we did not observe the secondary geyser (CS) erupting; however, sinter had accumulated around the vent, indicating that it was a preexisting feature. The mud volcano (MV) was a small fumarole in 2012. Most of the 2012 data at El Cobreloa and El Jefe geysers were previously reported by *Namiki et al.* [2014] and *Munoz-Saez et al.* [2015], respectively.

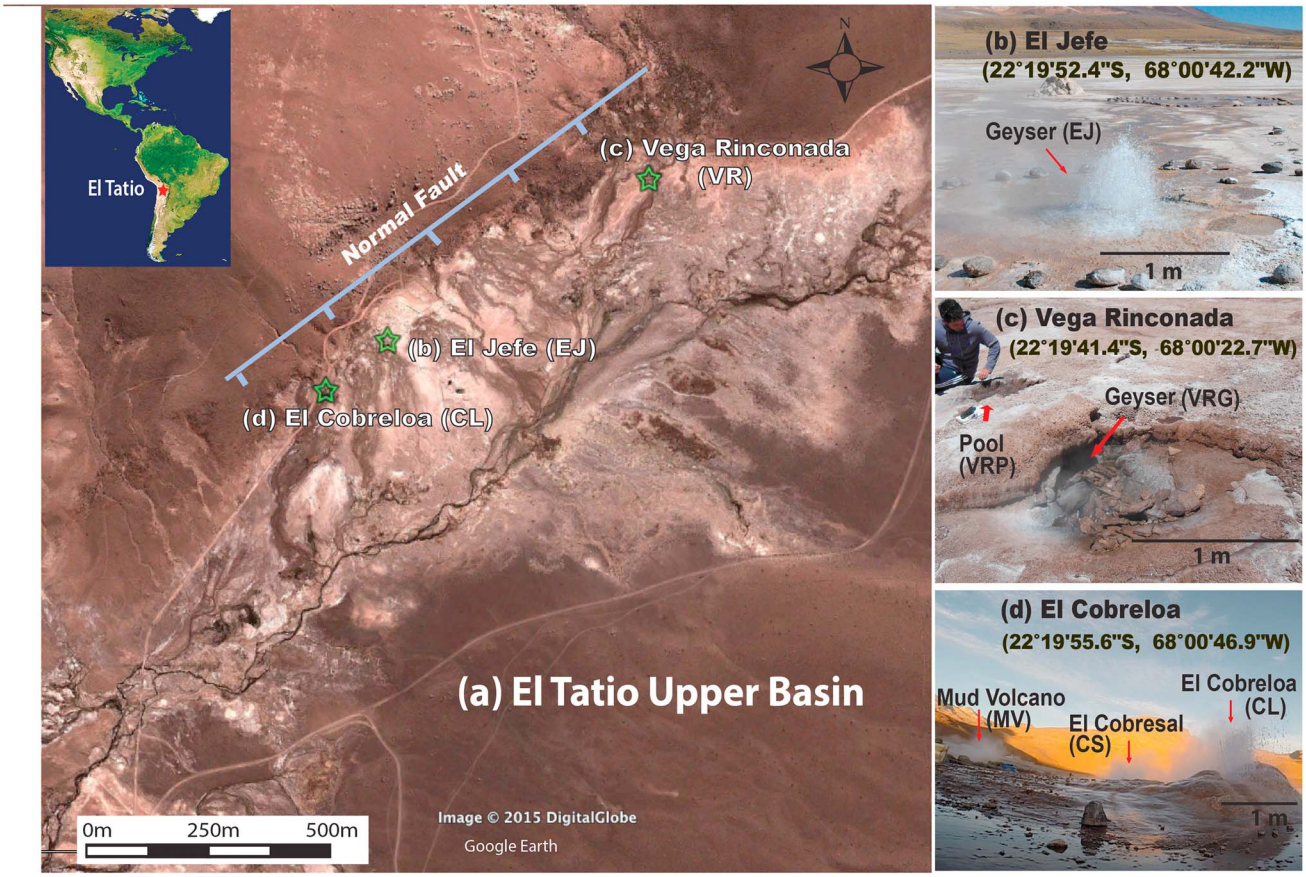

Figure 1. El Tatio Geyser Field: (a) Location (Google Earth, 2015); green stars indicate the positions of the studied geysers and the blue line indicates the normal fault that bounds the El Tatio half-graben, showing that geysers are located in the hanging wall of that fault. (b) El Jefe geyser (EJ) erupting in 2012, (c) Vega Rinconada geyser (VRG) and Vega Rinconada pool (VRP) in 2014, (d) El Cobreloa geyser (CL) is erupting in front, El Cobresal geyser (CS), and the mud pool steaming in the background in 2014.

2. El Tatio Geyser Field

The El Tatio geyser field is located in the Altiplano area of the Atacama Desert in the north of Chile (Figure 1a). The elevation of the area is 4.2 to 4.3 km above sea level, where the boiling temperature of water is approximately 86.6°C. El Tatio is the third largest geyser field in the world and includes more than 80 active geysers [*Glennon and Pfaff*, 2003]. The water supply for the geyser field is located 15 to 20 km to the east in the Bolivian Altiplano [*Lahsen*, 1976a, 1976b; *Cusicanqui et al.*, 1976; *Giggenbach*, 1978; *Munoz and Hamza*, 1993; *Cortecci et al.*, 2005]. The heat is provided by Holocene andesitic stratovolcanoes (with nonhistorical eruptions) that surround the geyser field [*Lahsen*, 1976a, 1976b]. Permeability is dominated by open fractures in the ignimbrite layers, according to data from geothermal wells [*Cusicanqui et al.*, 1975, 1976].

A north-south trending half-graben structure generates the El Tatio basin, which is filled with ~1 km of subhorizontal Miocene and Pliocene ignimbrites, tuffs, and lavas and covered by Holocene alluvial and glacial deposits [*Healy*, 1974; *Lahsen and Trujillo*, 1975]. Wells indicate that the geothermal reservoir is located in the highly fractured Pliocene ignimbrite Puripicar [*Cusicanqui et al.*, 1975, 1976], and the maximum temperature measured was 253°C [*Lahsen and Trujillo*, 1976]. Chemical and isotopic data from well and surface thermal waters suggest a complex mixing between magmatic, meteoric, and hydrothermal sources [*Cusicanqui et al.*, 1975; *Giggenbach*, 1978; *Tassi et al.*, 2005, 2010].

The El Jefe isolated geyser (EJ) (Figure 1b) has a sinter-lined conduit with a diameter of ~0.3 m near the surface, and the conduit narrows below a depth of 0.8 m; the maximum reachable depth was ~1.7 m in 2014. In the Vega Rinconada geyser-pool system (Figure 1c), the geyser (VRG) has a conduit ~10 cm in diameter that opens to a flared vent with a diameter of ~1 m and depth of 0.3 m. At depth, the conduit

narrows. Measurements with rods suggest that the conduit tilts ~30° from vertical, and our sensors extended down ~8 m (~7 m vertical depth). The pool (VRP) is a noneruptive hot spring with a diameter of ~0.5 m and is located 2 m away from the geyser. In the geyser-geyser-mud volcano system (Figure 1c), the primary geyser El Cobreloa (CL) has a small cone ~0.5 m high connected to the surface by a crack-lined vent. The maximum depth we could reach with instruments is ~1 m, at which point the conduit narrowed and twisted. The secondary geyser, El Cobresal (CS), is located ~8 m east of the primary geyser (CL) and has a conduit ~1.5 m deep and ~0.4 m in diameter. The mud volcano (MV) is located ~5 m north of the primary geyser (CL), and it lies in a surface depression ~2 m in diameter.

3. Field Measurements and Methodology

From 21–28 October 2012 and 2–9 October 2014, we obtained time series of video, ground deformation, temperature, and pressure. We synchronized the instruments and the data loggers with GPS clocks (GlobalSat BU-353 USB GPS Receiver and Scimolex SC-GPSCLK). For down-conduit measurements, we attached the sensors to a rigid metal rod to keep them in place.

3.1. El Jefe Geyser (EJ)

In 2012 at EJ we recorded surficial visible and infrared video and measured discharge, tilt, and surficial temperature. In the conduit, we recorded video, temperature, and pressure to a depth of 1.5 m [*Munoz-Saez et al.*, 2015]. In 2014, we measured temperature at the top of the conduit and at depths of 0.7 m, 1.2 m, and 1.7 m, using precalibrated K-type thermocouples connected to a QuadTemp 2000 (MadgeTech). The uncertainty in the temperature measurements is <1.1°C [*Omega Thermocouple Home Page*, n.d.]. At 1.7 m depth, we recorded pressure with a Honeywell pressure sensor (19C030PA4K) connected to a CR-850 (Campbell Scientific) data logger. The accuracy of the sensor is $<0.25\%$ of its range of 100 mV [*Honeywell Sensing and Control*, 2008], corresponding to ~95 Pa, for a temperature between 0°C and 82°C. All instruments recorded at 1 Hz frequency.

3.2. Vega Rinconada Geyser (VRG) and Pool (VRP)

In 2012 at VRG, temperature and pressure measurements were made inside the conduit. Eight evenly spaced sensors measured temperature from the surface to a depth of 7 m. Considering the conduit tilt, the corrected vertical depths are 0.0 m, 0.9 m, 1.7 m, 2.6 m, 3.5 m, 4.3 m, 5.2 m, and 6.1 m. We measured pressure during two eruptions at vertical depths of 4.3 m and 6.1 m. At VRP, we recorded temperature and pressure at a depth of 3 m for 3 days. We did not record pressure at VRP and VRG simultaneously.

In 2014, we installed a similar temperature array for 2 days, adding one pressure sensor at a vertical depth of 4.3 m. For the next 5 days, we recorded temperature 0.3 m above the surface (in the air) and at vertical depths of 0.9 m, 2.2 m, 3.5 m, 4.8 m, 5.6 m, and 6.3 m, with one pressure sensor added at 6.3 m. At VRP, we recorded pressure and temperature at a depth of 2 m for the entire period.

For temperature measurements, we used precalibrated K-type thermocouples connected to QuadTemp 2000 (MadgeTech) data loggers measuring at 1 Hz frequency. For pressure, we used Honeywell transducers (models 19C050PA4K and 19C030PA4K) mounted in watertight housings. In 2012, we connected the pressure sensors of VRG to a 24 bit Nanometrics Taurus logger recording with a frequency of 100 Hz. In 2014 the sensors were connected to a CR-1000x (Campbell Scientific) data logger recording with 1 Hz frequency. The pressure sensor in VRP was connected to a CR-1000x (Campbell Scientific), recording with a frequency of 1 Hz.

3.3. Primary Geyser Cobreloa (CL), Secondary Geyser Cobresal (CS), and Mud Volcano (MV)

In 2012 at CL we recorded surficial video and made surficial acoustic and temperature measurements [*Namiki et al.*, 2014]. In 2014, we recorded ground deformation with a tiltmeter located 3.5 m northwest of the vent. Pressure and temperature were measured in the geyser conduit at ~1 m depth, which is above water level while the geyser is quiescent. The temperature of water at the ground surface was measured 0.5 m northwest and 2.5 m west of the vent. At the CS geyser, we recorded video and measured temperature inside the conduit at depths of 0.0 m, 0.4 m, 0.8 m, and 1.2 m. At the MV, we recorded video on 8 October 2014 and measured temperature at the surface on 9 October 2014.

The instrumentation consisted of two digital video cameras with resolutions of 1440×1080 and 1920×1080 pixels recording 30 frames per second. The tiltmeter was calibrated to a resolution of $0.23\ \mu\text{rad mV}^{-1}$ (Applied Geomechanics Inc. Surface Mount Tiltmeter Model No. 701–2). At CL, the pressure

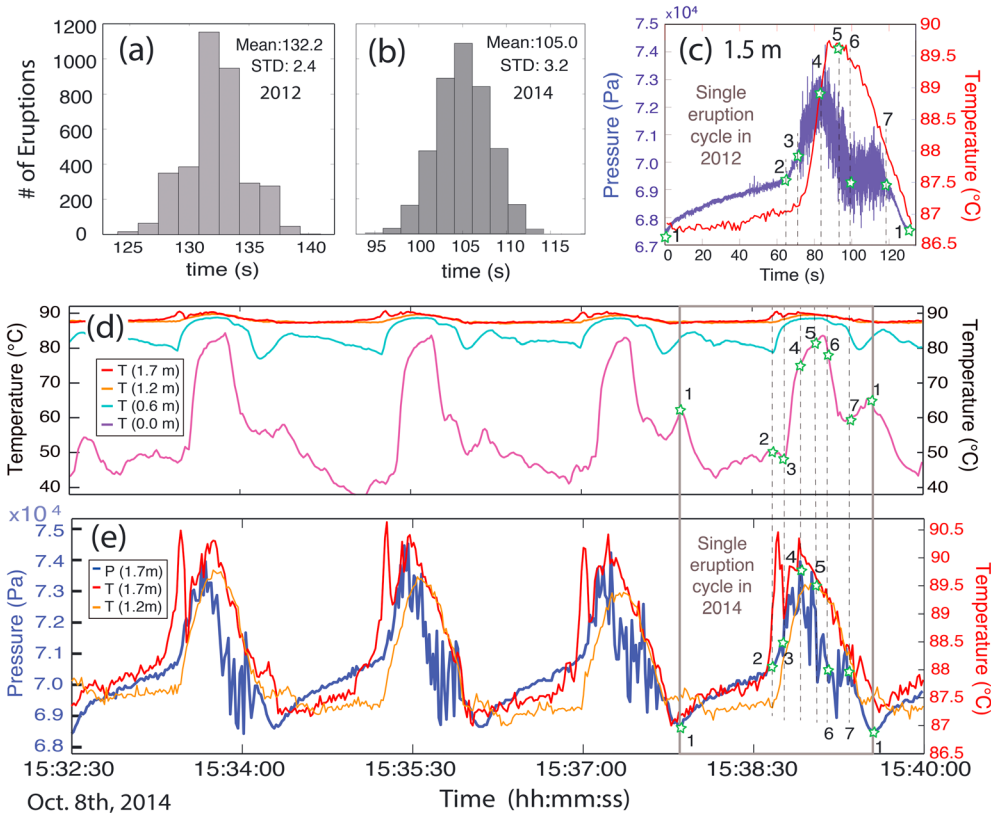

Figure 2. Eruption cycle of El Jefe geyser (EJ). (a) Histogram of interval between eruptions (IBE) for data collected in 2012 [*Munoz-Saez et al.*, 2015], showing a normal distribution with a mean of 132.2 s and standard deviation of 2.4 s. (b) IBE for 2014 with a mean of 105.5 s and standard deviation of 3.2 s. (c) Example of pressure and temperature evolution in 2012 at a depth of 1.5 m [*Munoz-Saez et al.*, 2015]; stars numbered 1 to 7 identify key stages in the cycle. (d) Time series of temperature at depths of 1.7 m (red), 1.2 m (orange), 0.6 m (light blue), and 0.0 m (pink) from 2014; subset of four eruption cycles. (e) Temperature at 1.7 m (red) and 1.2 m (orange), and pressure at 1.7 m (blue), during the same four cycles. The box at the right highlights a single eruption cycle, identifying key stages in the cycle identified from 2012 data (Figure 2c).

sensor XPM10 (the accuracy of the sensor is $<$0.25% of its range, corresponding to 100 Pa), K-type thermocouples, and the tiltmeter were connected to a HIOKI 8430 data logger recording at 100 Hz, though the response times of K-type thermocouples and the tiltmeter were longer than 10 ms. The temperature at CS was recorded every 1 s with a QuadTemp 2000 (MadgeTech) data logger. The pressure sensor located in the CS conduit leaked, and no data could be collected.

4. Results: Time Series

4.1. Isolated Geyser (EJ)

The evolution of both pressure and temperature at EJ is very similar between eruptions, and the interval between eruptions (IBE) is extremely regular (Figures 2a and 2b). Data from 2012 [*Munoz-Saez et al.*, 2015] showed that the eruption cycle at EJ has a mean IBE of 132.2 ± 2.4 s for 3531 eruptions (Figure 2a). In 2014 (Figures 2b, 2d, and 2e), the mean IBE decreased ~20%, to 105.0 ± 3.2 s for 4150 eruptions. This reduction reflected mostly the quiescent period, which decreased from 80 ± 3 s in 2012 [*Munoz-Saez et al.*, 2015] to 63 ± 4 s in 2014.

Based on 2012 data (Figure 2c), seven reference points in time identified different key stages in the eruption [*Munoz-Saez et al.*, 2015] and are also applicable to data from 2014 (Figures 2c–2e). Point 1 indicates the beginning of the geyser cycle; it coincides with the minimum water level and pressure inside the conduit (Figures 2c and 2e). The lower part of the conduit was underwater during the entire cycle (Figure 2e). Pressure increases from point 1 at 1.7 m, documenting refilling of the conduit. Point 2 marks the beginning of a rapid pressure increase (Figures 2c and 2e), which coincides with a rapid 2.5 to 3°C increase of temperature (Figure 2e). This change is detectable only at 1.7 m and was not observed in 2012 when measurements

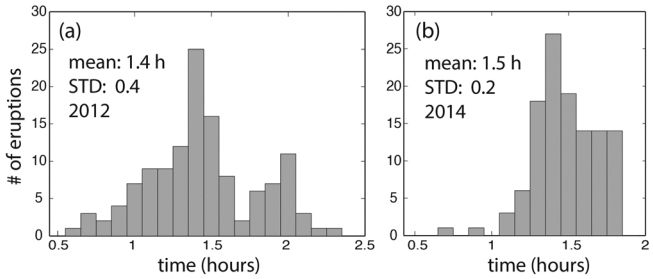

Figure 3. Interval between eruptions (IBE) for Vega Rinconada geyser (VRG) in (a) October 2012, showing a bimodal distribution centered at 1.4 h and 2.0 h, the mean IBE is 1.4 h and the standard deviation is 0.4 h, and (b) October 2014, showing an asymmetric distribution, centered at 1.4 h, the mean IBE is 1.5 h and the standard deviation is 0.2 h.

were restricted to depths less than 1.5 m. Temperature also starts increasing at 0.6 m (Figure 2d) when hot water reaches the sensor as the water level rises in the conduit. Point 3 indicates a sudden increase in pressure with large fluctuations (Figures 2c and 2e), and temperature increases in the entire conduit (Figures 2c–2e). Between points 3 and 4, water at 0.6 m reaches boiling conditions and the fountaining begins at the surface. Point 4 indicates the maximum pressure in the conduit (Figures 2c and 2e); after this point, pressure decreases at an approximately constant rate. Immediately after point 4, the temperature at 1.7 m has a second peak (Figure 2e), which occurs earlier than in the rest of the conduit and (again) was not detected in 2012 (Figure 2c). Point 5 indicates the maximum water temperature at 1.2 m, coincident with data from 2012, while pressure and temperature at 1.7 m are still decreasing. After this point, temperature at depths of 1.7 m, 1.2 m, and 0.6 m decreases at an approximately constant rate. At Point 6, the rate of pressure decrease changes, and this corresponds to the end of fountaining at the surface, which produces a rapid drop in the temperature in the upper part of the conduit, first at 0.0 m and then at 0.6 m (Figure 2d). Point 7 identifies the end of the pressure fluctuations, an increase in the rate of pressure decrease, and the end of the geyser cycle. After this point, erupted water returns to the conduit, increasing temperature in the upper part of the conduit, first at 0.0 m and then at 0.6 m (Figure 2d).

4.2. Geyser (VRG)-Pool (VRP)

The IBE analysis shows that the duration of eruption cycles changed from 2012 to 2014 (Figure 3), at least during the periods of measurements. However, the features of the cycles in both years are similar (Figure 4). In 2012, we measured 117 eruption cycles. The IBE varied from ~0.69 h to ~2.08 h, with a bimodal distribution centered at 1.4 h and 2 h for the major and minor peaks, respectively (Figure 3a), and a mean IBE of 1.4 ± 0.4 h (standard deviation). In 2014, we measured 118 eruption cycles. The IBE had less variability, from 0.75 h to 1.80 h. IBE values showed an asymmetric distribution centered at 1.4 h (Figure 3b), and the mean IBE was 1.5 ± 0.2 h. We calculated IBE using the local maximum of smoothed temperature measurements at 6.1 m depth as the beginning of an eruption and the local minimum at 0.9 m as the end of the eruption.

In both 2012 and 2014, pressures at different depths in the geyser conduit vary in the same way as pressure in the pool (Figures 4c and 4d). The temperature in the geyser changes at different depths, and over time (Figures 4b and 4c), while the temperature in the pool remains constant and below boiling point (~85°C) (Figure 4d). Cycles have different durations (Figure 3), but they have the same stages: a main eruption (Figure 4, A) and a quiescent period that can be divided in two stages, minor discharges of water (Figure 4, B) and water level changes at the conduit surface (Figure 4a).

During the main eruption (Figure 4, A), temperature increases in the deepest accessible part of the geyser conduit from ~90.5°C to 94°C (Figure 4b) and decreases in the middle part (3 to 5 m depth) from ~90.5°C to 89°C (Figures 4b and 4c). Pressure decreases at the beginning of the main eruption, levels out in the middle of the eruption, and then decreases again at the end of the eruption (Figures 4c and 4d). Both pressure drops produce large splashes of water at the surface (Figures 4a and 4c).

After the main eruption (Figure 4, B), during the first part of quiescent period, pressure increases irregularly, with two marked pressure drops of $\sim 0.5 \times 10^4$ Pa (Figure 4c) that coincide with small splashes or eruption of water at the surface (Figures 4a and 4c). Shorter eruption cycles have one or no pressure peaks during this period. In general, temperature tends to increase at an approximately steady rate of ~3.6°C/h throughout the conduit. In the deepest part of the conduit (Figure 4b), temperature shows some small peaks coincident with the pressure peaks. In the middle part of the conduit (3 to 4 m depth), the temperature drops somewhat,

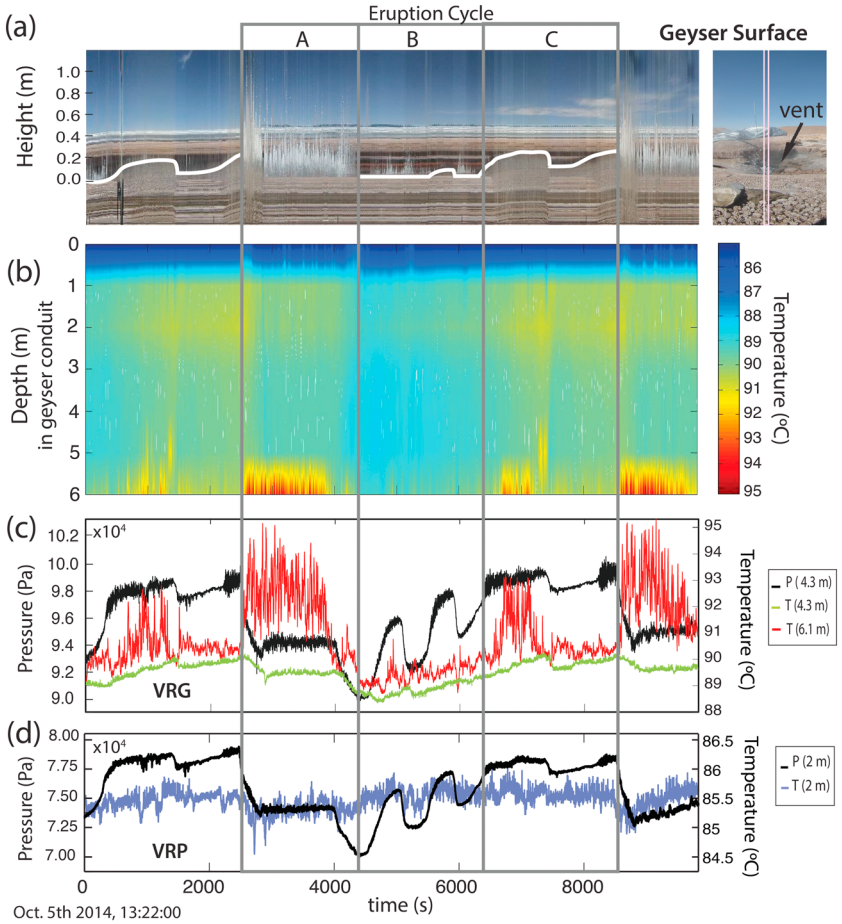

Figure 4. Vega Rinconada geyser (VRG) and pool (VRP) in 2014: (a) Right side shows a picture of the geyser surface, where we extract the central pixel for all heights (vertical pink line) for images taken every 1 s to obtain the surface time series shown on the left. White curve shows the liquid water height above the vent. Time interval "A" corresponds to the period of the main eruption, "B" to small discharges of water, and "C" to the increase of water level at the conduit surface measured from the image sequence. (b) Two-dimensional color plot of temperature inside the geyser conduit (temperature sensors were located at depths of 0.0 m, 0.9 m, 1.7 m, 2.6 m, 3.5 m, 4.3 m, 5.2 m, and 6.1 m) and temperature is interpolated between the measurement depths. (c) Time series of pressure (black) and temperature (green) at 4.3 m and 6.1 m (red) depths in the geyser conduit. (d) Time series of pressure (black) and temperature (blue) at 2 m depth in the pool. Time shown for all figures begins on 5 October 2014, 13:22:00 UTC.

following the changes in pressure (Figures 4b and 4c), and this region remains slightly colder than the rest of the conduit (Figure 4b).

During the second half of the quiescent period (Figure 4, C), pressure at depth increases and becomes constant (Figure 4c) while the conduit overflows at the surface (Figure 4a). At the same time, temperature in the deepest part of the conduit increases ~2°C (Figure 4b), followed by an increase of temperature in the rest of the conduit. After that, pressure drops again, ~0.2×10^4 Pa, water level drops at the surface, and temperature decreases in the middle of the conduit (Figures 4a–4c). Next, pressure increases as water level increases, and pressure becomes constant once the conduit overflows again. Temperature increases in the middle of the conduit until a new main eruption occurs.

4.3. Primary Geyser (CL), Secondary Geyser (CS), and MV

The CL geyser in 2012 was characterized by a main eruption every ~4.66 h, preceded by several minor eruptions every ~0.23 h [*Namiki et al.*, 2014]. The main eruption lasted ~1 h, started as liquid dominated, and evolved to steam dominated. Minor eruptions splashed hot water intermittently. We did not observe other time dependent features: CS was not erupting, and MV was a fumarole.

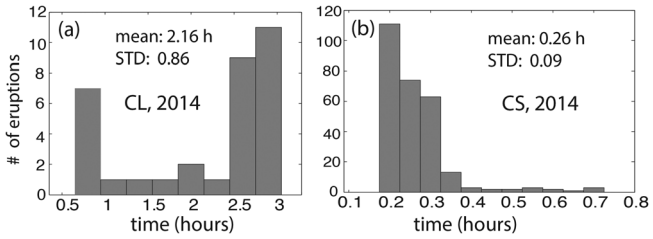

Figure 5. Interval between eruptions (IBE) of El Cobreloa geyser (CL) and El Cobresal geyser (CS) during October 2014. (a) For main eruptions in the CL, the IBE distribution is bimodal with peaks at 0.75 h and 2.75 h, the mean IBE is 2.16 h, and the standard deviation is 0.86 h. The IBE is calculated from signals in pressure, temperature, and tilt data. (b) The IBE of the CS shows an asymmetric distribution centered at 0.20 h; the mean IBE is 0.26 h and the standard deviation is 0.09 h. IBE is calculated from temperature measurements.

In 2014, CS and MV had intermittent eruptions, and eruptions of CL, CS, and MV are correlated (supporting information Movie S1). Minor eruptions of CL, and eruptions of CS, and MV occur at similar intervals. MV erupts just after the eruption of CS. During the steam-dominated eruption of CL, CS stops erupting. At the end of the first eruption of CS after the CL eruption, MV has a vigorous eruption that includes the ejection of pebbles.

We identified "main eruptions" from strong signals in the temperature, pressure, and tilt data. Compared with 2012, the main eruptions at CL were irregular and shorter, presenting a bimodal distribution of the IBE centered at 0.75 h and 2.75 h, the minor and major peaks, respectively (Figure 5a), for the 35 eruptions we measured. The mean IBE is ~2.16 h ± 0.86 h. Discharge of fluid during the eruptions lasted ~0.25 h to ~1 h depending on the duration of the cycle. Within main eruptions, we recognize small peaks in the temperature record inside the conduit that correspond to minor eruptions. Minor eruptions occur almost regularly, every ~0.24 h. We use video observations to confirm that these signals are associated with minor eruptions at the surface. For the secondary geyser CS, we measured 280 eruptions (Figure 5b). The IBE presents an asymmetric distribution centered at 0.2 h (Figure 5b), and the mean IBE was 0.26 ± 0.09 h. For the MV, we did not record enough eruptions to establish meaningful statistics.

At CL, during a main eruption, the temperature at 1 m depth in the conduit (Figures 6a and 6b) increases to 94°C, with one or more pulses. High temperature is sustained for several minutes and then temperature decreases steadily to ~85°C by the end of the eruption. Temperature at the geyser surface also increases (Figure 6a), as erupted water reaches the sensors deployed around the vent. The pressure in the conduit increases correspondingly (Figure 6b). By the end of the eruption, pressure decreases to a value close to atmospheric (6.1×10^4 Pa), indicating that the conduit is almost empty. The subatmospheric values of pressure can be attributed to noise and other pressure fluctuations coming from the empty conduit. The tilt (Figure 6c) increases at the beginning of an eruption but more slowly than the pressure signal. After the eruption, tilt in the radial direction decreases slowly. Throughout the minor eruptions (Figures 6b and 6d), temperature in the conduit (Figures 6a and 6b) increased to ~86.6°C (boiling point at atmospheric pressure). Minor eruptions of CL become progressively more vigorous following a main eruption of CL (Figure 6b), as *Namiki et al.* [2014] previously described for 2012 data, but not as systematically in 2014. Pressure tends to increase as temperature increases. When the geyser is not erupting, temperature is lower than 85°C, and pressure shows large amplitude and high-frequency variations about the atmospheric value (Figures 6b and 6d). There are no detectable tilt signals during minor eruptions (Figure 6c).

At CS geyser (Figure 7), we observe that when an eruption occurs the temperature increases sharply to 86–87°C in the entire conduit and maintains that value throughout the eruption. Once the eruption ends, the conduit empties and the temperature decreases below 50°C as erupted water pours back in the conduit. The duration of the eruption is almost the same in each cycle, but the quiescent period varies (Figure 7b). Temperature in the deepest part of the conduit (Figure 7a, 1.2 m) increases gradually as the conduit refills, and for longer quiescent periods the conduit refills more slowly before an eruption. The CS geyser stops erupting during the first maximum of temperature in the main eruption (Figures 6 and 7).

From temperature data (Figure 8), we observe that the temperature of MV is mostly maintained at a constant value close to the boiling point of water at the surface (86.6°C). Temperature in the MV (Figure 8) decreases at the beginning of the CS eruption and during minor eruptions of CL as liquid water flows to MV (supporting information Movie S1). We observed that the MV eruptions start at the end of the CS eruption (supporting information Movie S1), and the MV overflows during the main eruption of the CL (Figure 12).

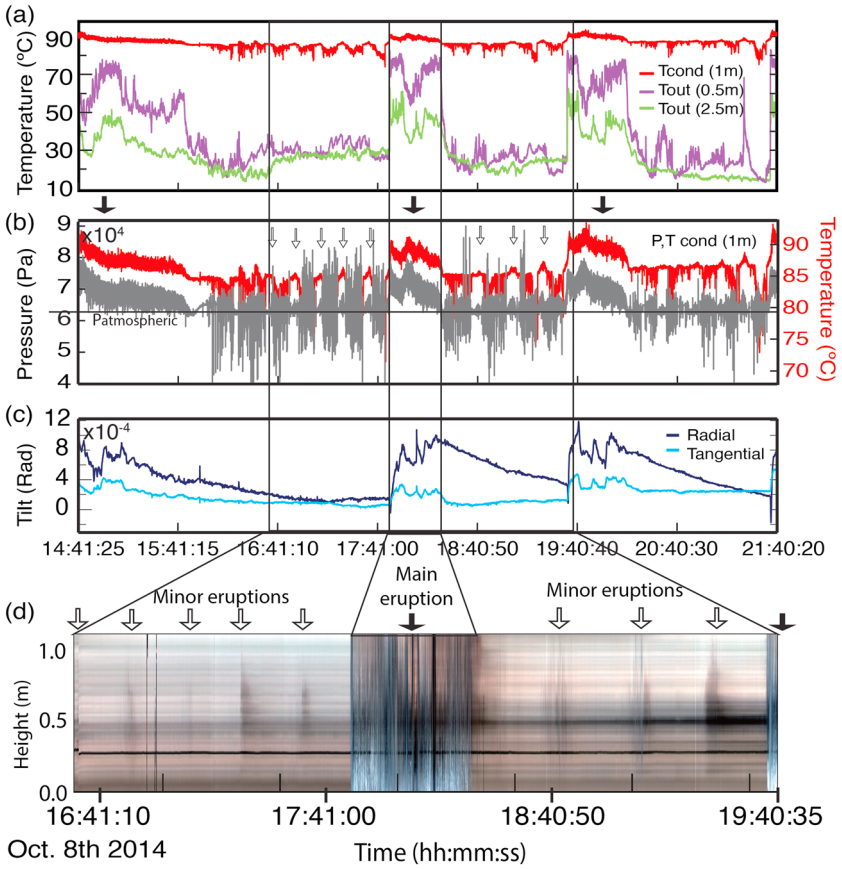

Figure 6. El Cobreloa (CL) showing an example of three eruption cycles measured on 8 October 2014. (a) Temperature at a depth of 1 m in the conduit (red) and horizontal distances of 0.5 m from the vent (purple), and 2.5 m from the vent. (b) Pressure (grey) and temperature (red) from sensors located at a depth of 1 m in the conduit. The black line indicates atmospheric pressure. (c) Ground deformation: tangential component (light blue) and radial component (dark blue). (d) Image sequence taken every 1 s above the geyser conduit, which corresponds to the part of the time series presented in Figures 6a and 6b; *y* axis indicates the height above the conduit. We observe water coming out of the conduit during minor eruptions (white arrows) and main eruptions (black arrow), also identified in Figure 6b.

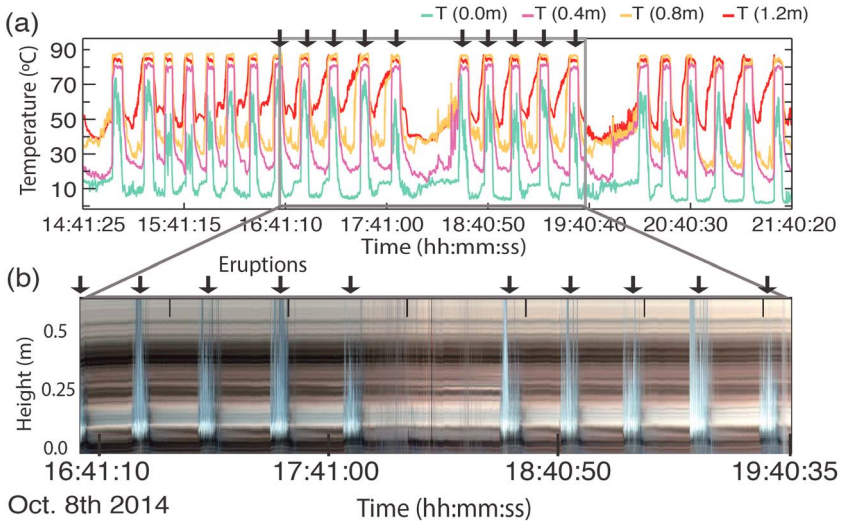

Figure 7. El Cobresal (CS) time series in 2014 (same interval as Figure 6). (a) Temperature in the conduit at depths of 0.0 m (green), 0.4 m (magenta), 0.8 m (yellow), and 1.2 m (red). (b) Images sequence taken every 1 s above the geyser conduit showing five consecutive eruptions (black arrow), followed by a quiet period, and then five more eruptions.

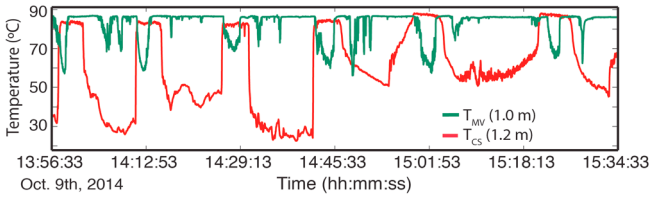

Figure 8. Temperature time series from 9 October 2014 at a depth of 1 m in the crater of the Mud Volcano (MV) shown in green and a depth of 1.2 m in El Cobresal conduit (CS) shown in red.

5. Discussion

5.1. Eruption Cycle

The geyser systems we studied present cycles of different complexity: the isolated geyser EJ has a single eruption per cycle, while VRG and the primary geyser CL have several minor eruptions preceding the main eruption. However, we recognize in all cases similar behaviors and eruption stages: recharge, preeruption, and eruption. The recharge is characterized by an increase of the hydrostatic pressure in the conduit as we observed at EJ (Figures 2 and 9, numbers 1 to 2) and VRG

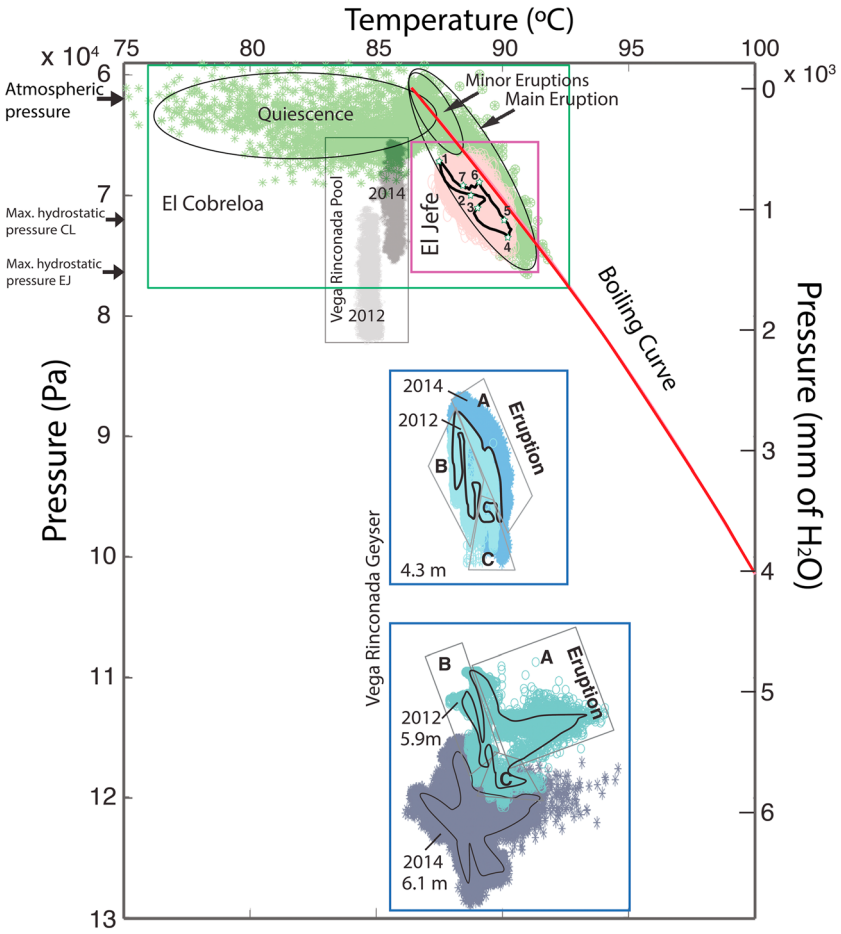

Figure 9. Temperature and pressure evolution within the geysers with the theoretical boiling curve for pure water (red curve). The *y* axis has two scales, at the left side we express pressure in Pa and at the right side relative pressure in millimeter of H_2O. In the purple box we plot data from 4150 eruptions of el Jefe (EJ) in 2014 at a depth of 1.7 m (pink dots), the black curve is the average during an eruption cycle, and numbers 1 to 7 indicate key points in the eruption cycle. In the green box, we plot data from 35 eruptions in 2014 at the primary geyser (CL) at a depth of 1 m (green circles); black ellipses show the quiescent period and the eruptions. Arrows on the left show the values of atmospheric pressure, and the theoretical maximum hydrostatic pressure measured in CL and EJ if the conduit is full of water. The green box shows that the pressure at CL exceeds the hydrostatic value during the main eruptions, but this does not occur for EJ. In the blue boxes, we plot data from Vega Rinconada geyser (VRG). In 2014 we measured 118 eruptions, and the sensors were located at depths of 4.3 m and 6.1 m. In 2012 we measured one eruption, and the sensors were located at depths of 4.3 m and 5.9 m. The black curve superimposed on the data shows the average pressure and temperature during one cycle. The letter A shows the evolution during main eruptions, B identifies the first part of the recharge period, and C shows the second half of the recharge period (as observed in Figure 4). In the grey box, we plot data of Vega Rinconada pool (VRP) from 2012 (light grey) and 2014 (dark grey).

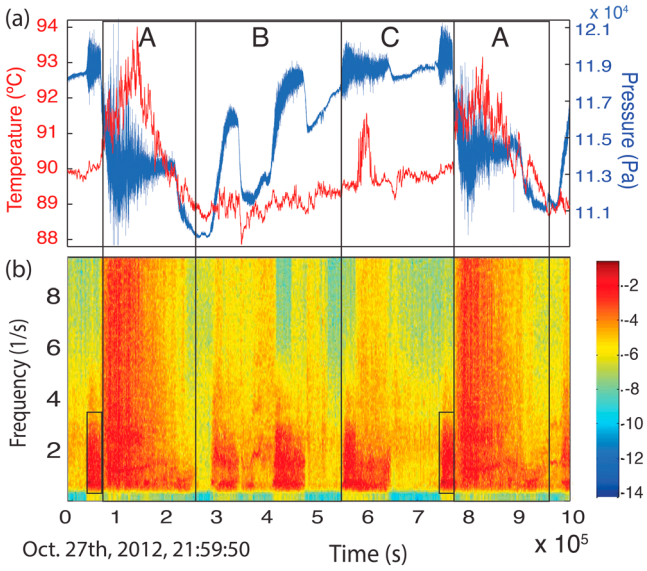

Figure 10. Eruption cycle of Vega Rinconada geyser (VRG). (a) Temperature (red) and pressure (blue) at a 5.9 m depth. Sampling frequency is 1 Hz for temperature, and 100 Hz for pressure. A corresponds to the main eruption, B and C to the recharge. (b) Spectrogram of the pressure during the same period of time. A 3.5 Hz signal occurs before every main eruption and during every local maximum of pressure during the recharge period. Time shown begins on 27 October 2012, 21:59:50 UTC.

(Figures 4 and 9, B and C). A preeruptive signal is observed in the pressure data before every eruption in EJ and VRG (Figure 10).

In CL geyser, the pressure during the quiescent period (Figure 9) is close to atmospheric values with temperatures below the boiling point, indicating that the conduit is empty at ~1 m, and we do not observe the recharge and preeruption signal. For the secondary geyser (CS), we observe recharge during the quiescent period (supporting information Movie S2). During an eruption (Figure 9) [*Munoz-Saez et al.*, 2015], the temperature and pressure follow the boiling curve, with no clear evidence of superheated fluid. At EJ and CL, we recorded pressure in the shallow conduit, which increases at the beginning of the eruption.

At EJ, pressure increases as the conduit fills during the liquid-dominated part of the eruption and never exceeds the hydrostatic pressure. In contrast, at CL, pressure exceeds hydrostatic values, suggesting that there is high-pressure steam within the conduit. As the eruption progresses, pressure and temperature decrease and follow the boiling curve as steam escapes from the vent and the conduit empties.

At VRG, we could reach depths well below the surface, providing insight into deeper parts of the geyser system. Pressure and temperature deeper than 4.3 m are below the boiling point during the entire cycle (Figure 9). This offset from the boiling curve occurs only at depth, given that the temperature in the upper part of the conduit is close to the boiling temperature at atmospheric pressure (~86°C, Figure 4b). At depth, pressure and temperature during the main eruption (Figure 9, A) evolve parallel to the boiling curve. Eruptions are initiated with a sudden increase of temperature and decrease in pressure, which can be attributed to the addition of steam. Addition of steam produces movement of fluid and decreases the density of the fluid above the sensor. Pressure in the pool VRP tracks that in the geyser VRG.

5.1.1. Recharge

From pressure data at EJ and VRG, we can estimate hydraulic parameters for the "aquifers" providing water to the conduit. During the quiescent period, the water level in the conduit of the isolated geyser EJ increases, which corresponds to changes in the hydraulic head $H(t)$ in the conduit. We assume that water drains from a deeper reservoir of constant hydraulic head H_∞ to the conduit with $H(t) < H_\infty$. The volumetric rate of refilling $S\frac{dH}{dt}$ (S is the cross section of a constant-radius conduit) is proportional to the head difference between the conduit and the reservoir:

$$S\frac{dH}{dt} = -g\alpha\,(H(t) - (H_\infty)), \tag{1}$$

where g is gravity, and α is the constant of proportionality that relates flow to head differences. By analogy to Darcy's law [*Steinberg et al.*, 1982; *Kedar et al.*, 1998; *Rudolph et al.*, 2012; *Munoz-Saez et al.*, 2015], α depends on the hydraulic parameters of the conduit and aquifer: hydraulic conductivity K, the distance L to the reservoir, and the surface area, A, over which recharge occurs. Hereafter, we define $H = 0$ to be the local ground surface.

Integrating equation (1), and applying the initial condition H_0 at $t = 0$, we obtain

$$H(t) = H_\infty + (H_\infty - H_0)\left(e^{\frac{-tag}{S}}\right). \tag{2}$$

Considering the depth of the sensor and transforming the measured pressure to hydraulic head by subtracting the atmospheric pressure and dividing pressure by density times gravity (ρg), we fit the data during the quiescent period and obtain for EJ in 2014: $H_{\infty\,EJ} = -0.82 \pm 0.05$ m, $H_{\infty\,EJ} - H_{0EJ} = 0.25 \pm 0.03$ m, $\left(\frac{S_{EJ}}{\alpha_{EJ} g}\right) = 33.90 \pm 4$ s. From the fit, we obtain $H_{0EJ} = -1.07 \pm 0.04$ m, which is consistent with the value obtained from the measured minimum pressure $H_{0\_data} = -1.03 \pm 0.05$ m. Using for S_{EJ} the cross section area for a conduit of radius 0.2 m, $\alpha_{EJ} = (4.30 \pm 0.60) \times 10^{-4}$ m s. From pressure data in 2012 [*Munoz-Saez et al.*, 2015], we obtain $H_{\infty\,2012} = -0.81 \pm 0.01$ m, $H_{0\_2012} = -1.02 \pm 0.01$ m, $\left(\frac{S_{2012}}{\alpha_{2012} g}\right) = 43.00 \pm 4.00$ s, and $\alpha_{2012} = (3.40 \pm 0.20) \times 10^{-4}$ m s. Parameters are similar in both years, indicating that the properties of the conduit and aquifer did not change significantly.

For VRG, the recharge of the conduit is interrupted by minor eruptions of water. Before every minor and main eruption, the pressure increases. Using equation (2) we can determine the evolution of hydraulic head documented by the pressure changes. We obtain $H_{\infty\,VR} = -0.02 \pm 0.07$ m. The parameter H_{0VR} increases from -1.06 ± 0.1 m to during the first part of the recharge (Figures 4, 9, and 10a period B) to -0.15 ± 0.05 m during the second part (Figures 4, 9, and 10a, period C), which is consistent with refilling of the conduit and successively higher initial water levels. The last term $\left(\frac{S_{VR}}{\alpha_{VR} g}\right)$ varies, reflecting changes in the geometry of the conduit; the parameter changes from 147 ± 15 s during the first part, where the conduit is being recharged (period B), to 345 ± 20 s during the second part, when the conduit overflows (Figure 4a, period C), and water accumulates in a wider depression at the surface. Considering αg constant, the conduit cross section (S) at depth may be half of the cross section at the surface.

Values of H_∞ within a couple meters of the local ground surface are similar to those inferred by active experiments performed at two geysers in Kamchatka [*Shteinberg et al.,* 2013]. High overpressures in a recharging reservoir thus do not appear necessary for geyser eruptions.

After the main eruption of CL, the radial component of the tilt decreases continuously, which requires continued subsurface movement of fluids. A porous conduit or a porous layer connecting different geyser conduits would permit circulation of fluids below the surface. Geysering wells show a very different evolution of tilt [*Nishimura et al.*, 2006; *Rudolph et al.*, 2012], with the tilt gradually increasing during the quiescent period. Conduits for artificial geysers are isolated pipes, and the measured ground deformation records fluid flow at the depth where the well is recharged. This hypothesis can explain the fact that the magnitude of the tilt signal is 1 order of magnitude larger than values reported at other natural geysers [*Munoz-Saez et al.*, 2015] and geysering wells [*Nishimura et al.*, 2006; *Rudolph et al.*, 2012]. The measured tilt near CL shows water recharge of shallow aquifers; in other instances, tilt reflects changes in deeper aquifers.

For the secondary geyser CS, during the recharge period (supporting information Movie S1) the water level increases, but in a discontinuous way, which we attribute to the influence of CL eruptions.

5.1.2. Preeruptive Behavior

By the end of recharge in the isolated EJ geyser, we observe a peak in temperature at 1.7 m in the 2014 data (Figures 2 and 9, points 2 to 3) that coincides with an increase in the rate of pressure change and with a 2 Hz preeruptive signal described in 2012 [*Munoz-Saez et al.*, 2015]. Similarly, in the geyser conduit of VRG, we identified a 3.5 Hz preeruptive signal preceding the main eruption and a 3.5 to 2 Hz signal when the pressure reaches a local maximum before every minor eruption (Figure 10). Some of those pressure peaks overlap with small temperature peaks in the deepest part of the conduit. Temperature peaks overlapping with the preeruption pressure fluctuations at EJ and VRG support the interpretation that steam bubbles are flowing into the conduit [*Mackenzie*, 1811; *Hutchinson et al.*, 1997; *Belousov et al.*, 2013; *Vandemeulebrouck et al.*, 2013; *Adelstein et al.*, 2014; *Munoz-Saez et al.*, 2015]. In down-conduit videos from CS (supporting information Movie S2), we observe sporadic addition of bubbles during the entire recharge period that intensified before the main eruption.

5.1.3. Liquid/Steam Distributions in the Conduit During Minor and Main Eruptions

The eruptions of the isolated geyser EJ (Figures 2c and 2e) and the primary geyser (CL) (Figure 5) started with a sudden increase of temperature and pressure, and both temperature and pressure decrease as the eruption progress. At EJ, pressure shows large fluctuations during an eruption (Figures 2c and 2e) that can be associated with boiling and bubble collapse [*Kedar et al.*, 1998; *Munoz-Saez et al.*, 2015; *Vandemeulebrouck et al.*, 2014]. Pressure never rises above the hydrostatic value for a liquid-filled conduit.

During minor eruptions at CL, the temperature of the water is close to boiling conditions at atmospheric pressure, whereas during the main eruption, pressure and temperature increase significantly and continue to follow the boiling curve (Figure 9). *Namiki et al.* [2014] show that boiling in the reservoir releases steam and hot liquid water to the conduit, causing minor eruptions, and heating the conduit. Eventually, the water becomes warm enough to boil, leading to a steam-dominated eruption that empties the conduit. During the field measurements in 2014, the sensor was located at a depth of 1 m. If the conduit was full of water, the hydrostatic pressure would be 10^4 Pa, greater than the atmospheric value. During the minor eruptions, pressure increases to this value (Figure 9), consistent with the conduit filling with liquid during a liquid-dominated eruption. During the main eruption, pressure exceeds the hydrostatic value (Figure 9), which can be attributed to increased vent pressure as steam is forced through the vent. During the steam-dominated part of the main eruption, only steam exists at the vent. The tilt of the surface follows pressure in the conduit, suggesting that water is supplied to the shallow aquifer by the main eruption. Pressure increases inside the conduit, and the ground rises in the direction of the vent, consistent with tilt measurements at other natural geysers such as EJ [*Munoz-Saez et al.*, 2015]. The very short, large amplitude tilt anomaly at the very beginning of each eruption is likely the poroelastic Noordbergum effect caused by faster propagation of mechanical deformation than hydraulic propagation of pressure changes, magnified where there are very compressible formations [*Kim and Parizek*, 1997].

Minor eruptions at VRG followed a single-step pressure drop in the conduit and a slight temperature increase at depth. The main eruption occurs during a two-step pressure drop that overlaps with a large peak in temperature in the deepest part of the conduit. We interpret the temperature increment in the deepest part of the conduit before and during an eruption as bubbles being released from a cavity or a boiling reservoir. Consequently, the pressure drops in the conduit due to liquid water moving down the conduit and fluid above the sensor becoming less dense owing to the addition of bubbles. The boiling temperature is reached in the upper part of the conduit (Figure 4b) where temperature is close to the local boiling temperature. According to the model fit during the recharge period (section 5.1.1) and visual observations (Figure 4), the conduit of VRG is full of water before the eruption begins, and then a large mass of water is removed from the conduit during the eruption and causes the decease of pressure. This also explains the opposite behavior of pressure in VRG, where pressure decreases at the beginning of an eruption. At EJ and CL, the upper part of the conduit was empty before the eruption and filled with water during an eruption, increasing the pressure.

The temperature in the middle of the conduit remains constant, suggesting that convection occurs in the conduit. Pressure decreases in the conduit would bring the upper part of the water column to boiling conditions if the water in the conduit were warm enough to boil at the surface. If bubble addition is sustained, a main eruption occurs and continues until steam is depleted. Otherwise, minor eruptions occur. Minor eruptions of water during the recharge are analogous to the preparation stage "preplay" that precedes the main eruptions characterized by pulses of liquid and/or steam discharge [e.g., *Kieffer*, 1984; *Karlstorm et al.*, 2013; *Namiki et al.*, 2014; *Adelstein et al.*, 2014], which can heat the conduit before a main eruption [*Namiki et al.*, 2014].

The magnitude of the pressure drops associated with minor eruptions ($\sim 0.5 \times 10^4$ Pa) is similar to each step in the main eruption, consistent with the idea of steam release from a bubble trap [e.g., *Belousov et al.*, 2013; *Vandemeulebrouck et al.*, 2013; *Adelstein et al.*, 2014; *Munoz-Saez et al.*, 2015] rather than fluid from a boiling reservoir [*Ingebritsen and Rojstaczer*, 1993, 1996; *Namiki et al.*, 2014], and provides insight into the size of the cavity. Considering the range of temperature in the upper conduit and the pressure dependence of the boiling temperature, water can boil from the surface to ~1 m depth during the minor eruptions and to ~2.5 m depth for main eruptions. In EJ, the eruption at the surface occurs between points 3 to 4 (Figures 2c–2e); and then the conduit decompresses and the boiling front propagates downward (Figures 2c–2e and Figure 9 between points 5 and 6). At both VRG and EJ, boiling occurs at the top of the water columns and boiling conditions propagate downward.

Given the depth of the heat input in the conduit, the bubble trap connected to VRG may be deeper than that at EJ. The eruption cycle (IBE) at VRG is longer and more irregular than EJ, because there is more water to warm up in the conduit, and multiple preplay or minor eruptions are needed to heat the conduit before the main eruption.

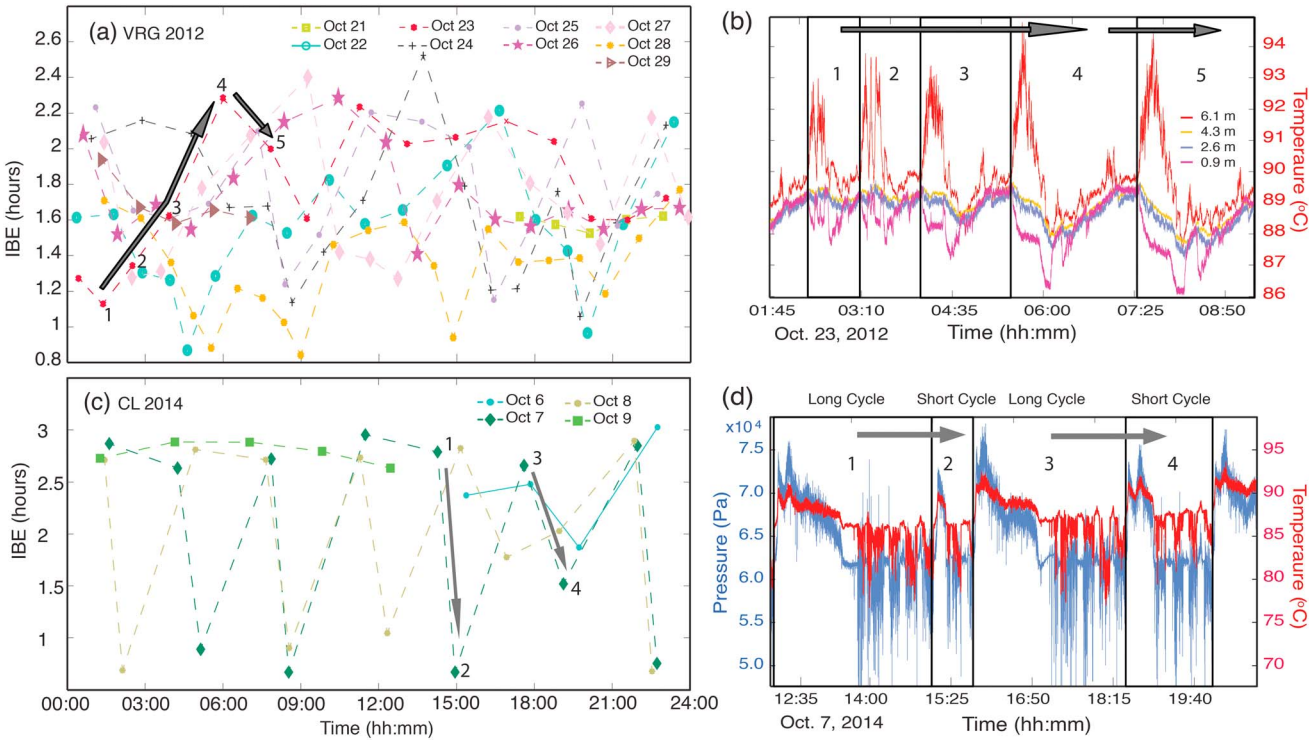

Figure 11. Interval Between Eruption (IBE) at Vega Rinconada geyser (VRG) and El Cobreloa geyser (CL). (a) IBE at different times of the day at VRG. Data from 21 October to 29 October 2012 are shown with different colors. (b) Temperature in VRG at depths of 0.9 m (dark magenta), 2.6 m (blue), 4.3 m (yellow), and 6.1 m (red). Boxes show five eruption cycles on 23 October 2012. Numbers from 1 to 4 and the long arrow on the red line ((Figure 11a) 23 October) shows the IBE increasing with time as in Figure 11b. From 4 to 5 the IBE decreases (short arrow). (c) IBE during the day for CL, data from 6 October to 9 October 2014. (d) Pressure (blue) and temperature (red) at a depth of 1 m in CL on 7 October 2014. From 1 to 2, and 3 to 4, the arrows in Figures 11c and 11d show a long eruption cycle followed by a short eruption cycle.

5.2. IBE and Interactions Between Geysers

5.2.1. Evolution Over Time

At EJ geyser, we observed a difference of ~20% in the IBE from 2012 to 2014 that is not associated with changes in recharge, but instead may be caused by changes in the supply of heat, changes in the bubble trap, or changes in the permeability of the surroundings [e.g., *Ingebritsen and Rojstaczer*, 1996]. In addition, changes in the IBE of CL from 2012 to 2014, the appearance of the two new eruptive features (CS and MV), and the change from bimodal (2012) to unimodal (2014) IBEs at VRG (Figure 3) highlight the dynamism and complexity of hydrological pathways. However, we cannot establish whether changes in IBE are caused by discrete events or instead occur progressively over time. For example, in February 2013, heavy rain fell in the area of San Pedro de Atacama, 70 km SW of El Tatio [*National Office of Emergency of the Interior Ministry, Chile*, 2013] and on 1 April 2014 a magnitude 8.2 earthquake occurred in Iquique, ~350 km NW of El Tatio [*United States Geological Service*, 2014]. Both of these events could potentially have affected the geysers given their magnitudes and locations [e.g., *Manga and Brodsky,* 2006; *Hurwitz et al.*, 2014; *Hurwitz and Lowenstern,* 2014]. Numerical simulations show that geyser cycles can be sensitive to changes in porosity, length and permeability of the conduit, permeability of the surrounding rock, and the rate of recharge [*Ingebritsen and Rojstaczer*, 1993, 1996]. Dynamic stress from distant earthquakes can modify permeability [e.g., *Manga et al.*, 2012] or the effective conduit length due to changes in the aperture of existing fractures [*Ingebritsen et al.*, 2006], and changes in recharge can be caused by climatic events. Depending on the orientation of fractures, reopening fractures can create connective pathways between geysers such as the CL, CS, and MV, reactivate a dormant geyser such as CS, and change the eruption behavior of a feature such as MV. Closing fractures can reduce the permeability and reduce the IBE, as documented at EJ. Switching from unimodal to bimodal eruption intervals has also been recognized at other geysers [e.g., *Silver and Valette-Silver*, 1992] and is not unexpected in hydrothermal systems where nonlinear relative permeability functions are sufficient to lead to switching [e.g., *Ingebritsen and Rojstaczer*, 1996].

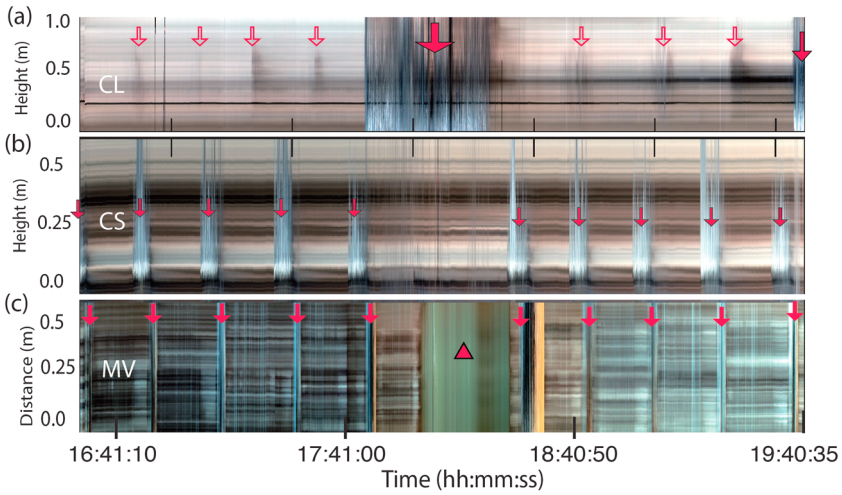

Figure 12. Image sequence during the same time period shown in Figures 6 and 7 of (a) El Cobreloa (CL), (b) El Cobresal (CS), and (c) Mud volcano (MV). For Figures 12a and 12b, pictures were taken facing the water column; in Figure 12c, the pictures were taken facing toward the MV vent. Red arrows indicate the eruptions, and the triangle in Figure 12c shows the MV overflowing.

VRG in 2012 and CL in 2014 have bimodal distributions of the IBE (Figures 3a and 5a). Changes in the IBE have been attributed to changes in the air temperature [*Hurwitz et al.*, 2008, 2014; *Merzhanov et al.*, 1990] and stresses induced by barometric pressure changes (3×10^2 Pa) and solid Earth tides (10^3 Pa) [*Hutchinson et al.*, 1997; *Vandemeulebrouck et al.*, 2013], which occur in daily cycles. In VRG and CL, long and short eruption cycles occur independent of the time of the day (Figures 11a and 11c), indicating that the bimodality of those geysers is not the consequence of environmental perturbations. At VRG (Figures 11a and 11b), several short eruptions can occur before a long eruption, and the IBE increases progressively until a long eruption occurs; after that, IBE decreases progressively. Preplay or minor eruptions are absent during the recharge as cycles become shorter. In CL, short and long eruptions cycles usually alternate (Figures 11c and 11d). Short cycles may be heating the conduit before a long eruption and could be considered very large preplay events.

5.2.2. Geyser-Geyser Interaction

The time series (Figures 6–8) and surface observations (Figure 12 and supporting information Movie S1) document the interaction between three eruptive features (CL, CS, and MV), suggesting that a permeable "aquifer" connects all three. As we discussed in section 5.1.3, pressures inside the conduits fluctuate, which leads to water transport between eruptive features. Here we summarize possible mechanisms for the observed interaction.

As pressure increases in the CL conduit by water recharge, water in a shallow aquifer is sent to the other features. The shallow water is below boiling point, suppressing the eruption of the secondary geyser CS (Figure 12 and the longer quiescent period in Figure 13b), and overflowing the MV (Figure 12). As the CL conduit fills with steam, the pressure below the vent in the deeper conduit decreases, and water in the aquifer may flow back toward the CL conduit.

Pressure in the conduit of CS may increase at the beginning of the eruption when the conduit fills with water, as occurs at EJ, sending some liquid back to CL and to the MV. This liquid can produce temporarily liquid-dominated stages during the main eruption of CL (Figures 13a and 13b) and decreases the temperature of the MV (Figure 8), suppressing its eruption. By the end of the CS eruption, pressure in the conduit becomes low, allowing liquid to flow back to CS and allowing MV to erupt (Figure 8 and supporting information Movie S1). The aquifer connecting the geysers must be deep enough (at least a few tens of centimeters) that it does not sense diurnal variations in temperature. But it must be shallow enough to sense pressure changes in the geyser conduits. The fluid supply from the deeper sources may also be influenced by pressures in the geyser conduits. Some combination of all these factors control the complex interaction among the three eruptive features.

The periodic eruptions and variations of pressure in the conduit will lead to periodic variations in pore pressure in the porous materials surrounding the geyser. These pressure variations decay exponentially in magnitude with

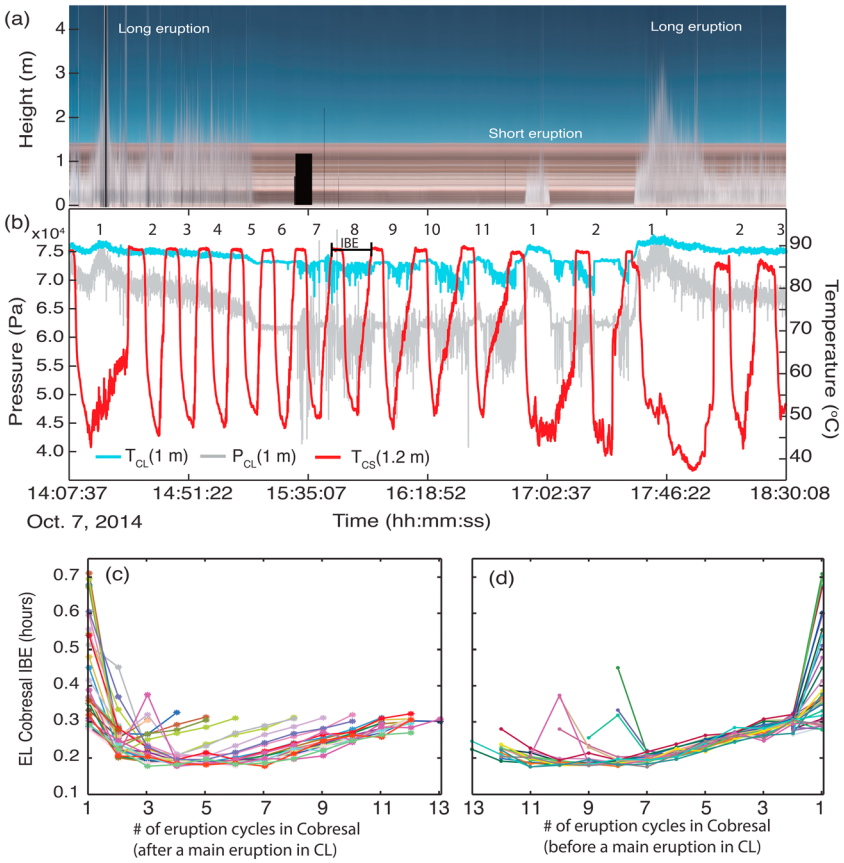

Figure 13. Interaction between El Cobreloa geyser (CL) and El Cobresal geyser (CS). (a) Time series of surface expression of eruptions showing three main eruptions at CL. (b) Time series of temperature (light blue), pressure (grey) of CL at 1 m depth, and temperature in CS at 1.2 m depth (red) during the same time period of Figure 13a. Main eruptions of CL are characterized by a large increase of temperature and pressure that correlate with water height in Figure 13a. In the time series of CS, we numbered each eruption interval sequentially. Number 1 has a large IBE that coincides with a main eruption of CL. (c) IBE of eruptions at CS geyser during one cycle of CL as we observe in Figure 13b. We observe that the IBE of CS decreases at the beginning of the CL eruption cycle, and then increases over time. (d) IBE of eruptions at CS geyser before the main eruption of CL; number 1 corresponds to the longest cycle, and previous eruptions are numbered sequentially.

increasing distance from the geyser, decreasing by a factor of e over distance $L_c \sim \sqrt{DT}$, where D is the hydraulic diffusivity and T is the interval between eruption. We infer that the separation of thermal features d is small enough compared to L_c that pressure fluctuations can influence eruptions, that is $d < O(L_c)$. The hydraulic diffusivity $D = \frac{k}{\mu(\beta_1 + \phi\beta_2)}$ depends on the permeability (k), viscosity of water ($\mu = 0.335 \times 10^{-3}$ Pa s, near the boiling temperature), compressibility of the rock (β_1) and liquid water (β_2), and porosity (ϕ); $\beta_1 + \phi\beta_2$ is $\sim 10^{-10}\,\mathrm{Pa}^{-1}$. Given the mean IBE of CL ~ 2.16 h, and that the separation of CS and CL is ~8 m, a permeability $k > 10^{-16}\,\mathrm{m}^2$ should allow pressure fluctuations from one geyser to be sensed at the other. The isolated geyser EJ is located 165 m from CL, so that a permeability $k > 10^{-13}\,\mathrm{m}^2$ would be needed for an interaction between those geysers. EJ seems to be unresponsive to the other geysers, thus bounding permeability.

5.2.3. Geyser-Pool Interaction

Similar changes in pressure in VRG and VRP indicate strong hydrologic connections between the pool and the geyser though a permeable zone. The temperature evolves differently between the pool and the geyser: in VRP the temperature remains constant, while in VRG it varies throughout the geyser cycle, suggesting that the heat source is only directly connected to the geyser conduit. A temperature decrease in the upper part of the geyser conduit, after the pressure decreases, can be attributed to the permeable zone draining colder water into the geyser conduit. The addition of colder water could contribute to ending the eruption. We do not observe warmer water flowing from the geyser to the pool during the eruption, indicating that flux between eruptions is a small fraction of the pool volume.

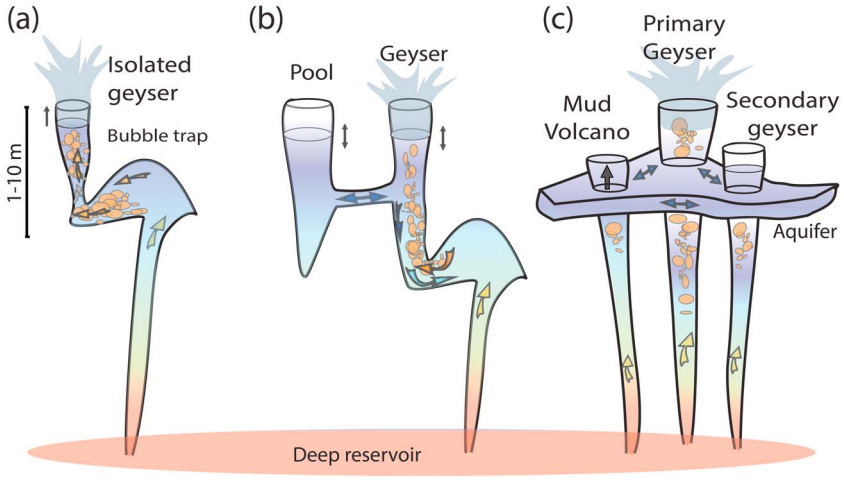

Figure 14. Conceptual model for the three geyser systems. (a) The isolated geyser, El Jefe (EJ), has a single conduit connected to the bubble trap. Bubbles moving toward the conduit indicated by the arrows generate the eruption. (b) Vega Rinconada, the geyser (VRG)-pool (VRP) system, has two connected conduits, but only the geyser is connected to the bubble trap. Arrows show the direction of fluid flow. (c) El Cobreloa (CL), El Cobresal (CS), and the Mud Volcano (MV) are three conduits connected through a permeable layer or aquifer.

5.3. Conceptual Model

For the single geyser (EJ), episodic addition of heat from below (e.g., a bubble trap) increases the temperature in the upper part of conduit (Figure 14). When the water reaches boiling conditions, the geyser erupts. Eruptions are frequent (~2 min) and without preplay.

The geyser (VRG) and the pool (VRP) are hydraulically well connected. However, addition of heat occurs only in the deepest part of the conduit (Figure 14). The bubble trap may be deeper compared to EJ geyser, the IBE is longer, and multiple preplays or minor eruptions heat the conduit before the main eruption. During the main eruption, the bubble trap empties, causing flow of liquid water into the cavity, which decreases pressure in the conduit and the pool.

The two geysers (CL and CS) and the mud volcano (MV) are hydraulically connected through a permeable aquifer (Figure 14). These all may be connected to a deeper heat source. The main geyser (CL) and the secondary geyser (CS) interact, and both control the periodicity of the MV.

6. Conclusion

Our field measurements document that geyser systems evolve over time, including changes in interval between eruption (IBE) and development of new thermal features. These measurements allow us to answer some of the questions highlighted in section 1:

1. How is the eruption cycle of a geyser influenced by other adjacent and distant thermal sources? Are hot springs and geysers connected through permeable pathways? Geysers can be connected through permeable pathways to other nearby hot springs and geysers. Distances must be small enough that pressure changes in one geyser can be sensed at the other geysers. At El Tatio, reasonable permeabilities are inferred based on the separation distance of interacting and noninteracting geysers.
2. Why do so few hot springs erupt as geysers? Given enough heat and water, the right subsurface geometry may be necessary. Geysers with deeper bubble traps and greater volume are more likely to have preplay or minor eruptions. Complexity in the underground geometry determines the features of the eruption cycles.

Acknowledgments
This research was supported by National Science Foundation (EAR1114184), CEGA-University of Chile, Conicyt-Chile, Center for Latin American Studies-University of California Berkeley, and the Judy Webb Chair at University of California, Berkeley. We thank the El Tatio team who provided essential help in the laboratory and in the field: Fred Murphy, Shaul Hurwitz, Max Rudolph, Chi-Yuen Wang, Ameeta Patel, Eric King, Angello Negri, Pablo Ortega, Alberto Ardid, Camilo Sanchez, Martin Reich, Cyndi Kelly, and Sarah Barrett. The fieldwork was performed with the permission of the Amayras Communities of Caspana and Toconce. Takeshi Matsushima, Jun Oikawa, and Atsushi Watanabe helped us with the tilt measurements. We thank the Editors and reviewers for helping to clarify the results and interpretations. Both the data and input files necessary to reproduce the figures are available from the authors upon request (carolimunoz@berkeley.edu, mmanga@berkeley.edu, and namiki@hiroshima-u.ac.jp). Any use of trade, firm, or product names is for descriptive purposes only and does not imply endorsement by the University of California or the authors.

References

Adelstein, E., A. Tran, C. Muñoz-Saez, A. Shteinberg, and M. Manga (2014), Geyser preplay and eruption in a laboratory model with a bubble trap, *J. Volcanol. Geoth. Res.*, *285*, 129–135.

Belousov, A., M. Belousova, and A. Nechayev (2013), Video observations inside conduits of erupting geysers in Kamchatka, Russia, and their geological framework: Implications for the geyser mechanism, *Geology*, *41*, 387–390, doi:10.1130/G33366.1.

Cortecci, G., T. Boschetti, M. Mussi, C. H. Lameli, C. Mucchino, and M. Barbieri (2005), New chemical and original isotopic data on waters from El Tatio geothermal field, northern Chile, *Geochem. J.*, *39*(6), 547–571.
Cusicanqui, H., W. A. J. Mahon, and A. J. Ellis (1975), The geochemistry of the El Tatio geothermal field, Northern Chile, Second United Nations Symposium on the Development and Utilization of Geothermal Resources, 703–711, San Francisco.
Cusicanqui, H., W. A. J. Mahon, and A. J. Ellis (1976), The geochemistry of the El Tatio geothermal field, northern Chile, in *Proceedings, 2nd U.N. Symposium on Geothermal Fields*, pp. 140–156, Berkeley, Calif.
Fournier, R. O. (1969), Old Faithful: A physical model, *Science*, *163*, 304–305.
Giggenbach, W. F. (1978), The isotopic composition of waters from the El Tatio geothermal field, Northern Chile, *Geochim. Cosmochim. Acta*, *42*, 979–988.
Glennon, J. A., and R. M. Pfaff (2003), The extraordinary thermal activity of El Tatio Geyser Field, Antofagasta Region, Chile, *GOSA Trans.*, *8*, 31–78.
Healy, J. (1974), Geological report on El Tatio geothermal field, Antofagasta province, Chile, UNDP-Report.
Honeywell Sensing and Control (2008), Web. [Available at http://images.vnsky.com/upfile/pdf/2013020904/55a6fbb8-0f96-42f8-8ca1-fc646537bfea.pdf, accessed on 09 Sept. 2015.]
Hurwitz, S., and J. B. Lowenstern (2014), Dynamics of the Yellowstone hydrothermal system, *Rev. Geophys.*, *51*, 375–411, doi:10.1002/2014RG000452.
Hurwitz, S., A. Kumar, R. Taylor, and H. Heasler (2008), Climate-induced variations of geyser periodicity in Yellowstone National Park, USA, *Geology*, *36*, 451–454.
Hurwitz, S., R. A. Sohn, K. Luttrell, and M. Manga (2014), Triggering and modulation of geyser eruptions in Yellowstone National Park by earthquakes, Earth tides, and weather, *J. Geophys. Res. Solid Earth*, *119*, 1718–1737, doi:10.1002/2013JB010803.
Hutchinson, R. A., J. A. Westphal, and S. W. Kieffer (1997), In situ observations of Old Faithful Geyser, *Geology*, *25*, 875–878.
Ingebritsen, S. E., and S. A. Rojstaczer (1993), Controls on geyser periodicity, *Science*, *262*, 889–892, doi:10.1126/science.262.5135.889.
Ingebritsen, S. E., and S. A. Rojstaczer (1996), Geyser periodicity and the response of geysers to deformation, *J. Geophys. Res.*, *101*, 21,891–21,905, doi:10.1029/96JB02285.
Ingebritsen, S. E., W. E. Sanford, and C. E. Neuzil (2006), *Groundwater in Geologic Processes*, 2nd ed., 536 pp., Cambridge Univ. Press, Cambridge.
Karlstorm, L., S. Hurwitz, R. A. Sohn, J. Vandemeulebrouck, F. Murphy, M. L. Rudolph, M. J. S. Johnston, M. Manga, and R. B. McCleskey (2013), Eruptions at Lone Star Geyser, Yellowstone National Park, USA, Part 1: Energetics and eruption dynamics, *J. Geophys. Res. Solid Earth*, *118*, 1–15, doi:10.1002/jgrb.50251.
Kedar, S., H. Kanamori, and B. Sturtevant (1998), Bubble collapse as the source of harmonic tremor at Old Faithful Geyser, *J. Geophys. Res.*, *103*, 24,283–24,299, doi:10.1029/98JB01824.
Kieffer, S. W. (1984), Seismicity at Old Faithful Geyser: An isolated source of geothermal noise and possible analogue of volcanic seismicity, *J. Volcanol. Geotherm. Res.*, *22*, 59–95.
Kieffer, S. W. (1989), Geologic nozzles, *Rev. Geophys*, *27*, 3–38, doi:10.1029/RG027i001p00003.
Kim, J. M., and R. R. Parizek (1997), Numerical simulation of the Noordbergum effect resulting from groundwater pumping in a layered aquifer system, *J. Hydrol.*, *202*, 231–243, doi:10.1016/S0022-1694(97)00067-X.
Kiryukhin, A. V., T. V. Rychkova, and I. K. Dubrovskaya (2012), Formation of the hydrothermal system in Geysers Valley (Kronotsky Nature Reserve, Kamchatka) and triggers of the giant landslide, *Appl. Geochem.*, *27*, 1753–1766, doi:10.1016/j.apgeochem.2012.02.011.
Lahsen, A. (1976a), La actividad geotermal y sus relaciones con la tectónica y el volcanismo en el norte de Chile, I Congreso Geológico Chileno, Actas, B105 – B127, Antofagasta.
Lahsen, A. (1976b), Geothermal exploration in Northern Chile-Summary, *Circum Pacific Energy and Mineral Resour. Conf.*, pp. 169–175, Honolulu.
Lahsen, A., and P. Trujillo (1975), El Tatio Geothermal Field, in *Proceedings of the Second United Nations Symposium on the Development and Use of Geothermal Resources*, pp. 157–178, San Francisco, Calif., 20–29 May.
Lahsen, A., and P. Trujillo (1976), El campo geotermico de El Tatio, Chile, Proyecto Geotermico CORFU-ONU, Internal Rep.
Mackenzie, G. (1811), *Travels in the Island of Iceland, Edinburgh*, vol. 27, Alam and Company, Edinburgh.
Manga, M., and E. E. Brodsky (2006), Seismic triggering of eruptions in the far field: Volcanoes and geysers, *Annu. Rev. Earth Planet. Sci.*, *34*, 263–291.
Manga, M., I. Beresnev, E. E. Brodsky, J. E. Elkhoury, D. Elsworth, S. E. Ingebritsen, D. C. Mays, and C.-Y. Wang (2012), Changes in permeability by transient stresses: Field observations, experiments and mechanisms, *Rev. Geophys.*, *50*, RG2004, doi:10.1029/2011RG000382.
Merzhanov, A. G., A. S. Shteinberg, and G. S. Shteinberg (1990), Heat and mass exchange in geyser systems, in *Proceedings of the 9th International Heat Transfer Conference*, edited by G. Hestroni, pp. 323–328.
Munoz, M., and V. Hamza (1993), Heat flow and temperature gradients in Chile, *Stud. Geophys. Geod.*, *37*, 315–348.
Munoz-Saez, C., M. Manga, S. Hurwitz, M. Rudolph, A. Namiki, and C.-Y. Wang (2015), Dynamics within geyser conduits, and sensitivity to environmental perturbations: Insights from a periodic geyser in the El Tatio geyser field, Atacama Desert, Chile, *J. Volcanol. Geotherm. Res.*, *292*, 41–55, doi:10.1016/j.jvolgeores.2015.01.002.
Namiki, A., C. Munoz-Saez, and M. Manga (2014), El Cobreloa: A geyser with two distinct eruption styles, *J. Geophys. Res. Solid Earth*, *119*, 6229–6248, doi:10.1002/2014JB11009.
National Office of Emergency of the Interior Ministry, Chile (2013), Monitoreo actualizado de Alerta Roja Comunal por precipitaciones en San Pedro de Atacama, Web, 7 Feb. [Available at http://www.onemi.cl/informate/monitoreo-actualizado-de-alerta-roja-comunal-por-precipitaciones-en-san-pedro-de-atacama/.]
Nishimura, T., M. Ichihara, and S. Ueki (2006), Investigation of the Onikobe geyser, NE Japan, by observing the ground tilt and flow parameters, *Earth Planets Space*, *58*, e21–e24.
Omega Thermocouple Home Page. Thermocouple Probes, n.d. Web. [Available at http://www.omega.com/thermocouples.html, accessed on 09 Sept. 2015.]
Rojstaczer, S., D. L. Galloway, S. E. Ingebritsen, and D. M. Rubin (2003), Variability in geyser eruptive timing and its causes: Yellowstone National Park, *Geophys. Res. Lett.*, *30*(18), 1953, doi:10.1029/2003GL017853.
Rudolph, M. L., M. Manga, S. Hurwitz, M. J. Johnston, L. Karlstrom, and C.-Y. Wang (2012), Mechanics of Old Faithful Geyser, Calistoga, California, *Geophys. Res. Lett.*, *39*, L24308, doi:10.1029/2012GL054012.
Scott, B. J. (1992), Characteristics of cyclic activity in Frying Pan and Inferno Crater Lakes, Waimangu, paper presented at 14th New Zealand Geothermal Workshop, Geothermal Institute, University of Auckland, Auckland, New Zealand.
Scott, B. J. (1994), Cyclic activity in the crater lakes of Waimangu hydrothermal system, New Zealand, *Geothermics*, *23*, 555–572.

Shteinberg, A., M. Manga, and E. Korolev (2013), Measuring pressure in the source region for geysers, Geyser Valley, Kamchatka, *J. Volcanol. Geotherm. Res.*, *264*, 12–16.

Silver, P., and N. J. Valette-Silver (1992), Detection of hydrothermal precursors to large northern California earthquakes, *Science*, *257*, 1363–1368.

Steinberg, G. S., A. G. Merzhanov, and A. S. Steinberg (1982), Geyser process: Its theory, modeling and field experiment. Part 4. On seismic influence on geyser regime, *Mod. Geol.*, *8*, 79–86.

Tassi, F., C. Martinez, O. Vaselli, B. Capaccioni, and J. Viramonte (2005), Light hydrocarbons as redox and temperature indicators in the geothermal field of El Tatio (northern Chile), *Appl. Geochem.*, *20*, 2049–2062.

Tassi, F., F. Aguilera, T. Darrah, O. Vaselli, B. Capaccioni, R. J. Poreda, and A. Delgado Huertas (2010), Fluid geochemistry of hydrothermal systems in the Arica-Parinacota, Tarapacá and Antofagasta regions (northern Chile), *J. Volcanol. Geotherm. Res.*, *192*, 1–15.

United States Geological Service (2014), M8.2–94 km NW of Iquique, Chile, Web. [Available at http://earthquake.usgs.gov/earthquakes/eventpage/usc000nzvd#general_summary, accessed on April 1, 2014.]

Vandemeulebrouck, J., P. Roux, and E. Cros (2013), The plumbing of Old Faithful Geyser revealed by hydrothermal tremor, *Geophys. Res. Lett.*, *40*, 1989–1993, doi:10.1002/grl.50422.

Vandemeulebrouck, J., R. A. Sohn, M. L. Rudolph, S. Hurwitz, M. Manga, M. S. J. Johnston, S. A. Soule, J. M. G. Glen, L. Karlstrom, and F. Murphy (2014), Eruptions at Lone Star Geyser, Yellowstone National Park, USA, Part 2: Constraints on subsurface dynamics, *J. Geophys. Res. Solid Earth*, *119*, 8688–8707, doi:10.1002/2014JB011526.

White, D. E. (1967), Some principles of geyser activity, mainly from Steamboat Springs, Nevada, *Am. J. Sci.*, *265*, 641–684.